UCRL-JC-123751
PREPRINT
CONF-9604147--2

RK-TBA Prototype RF Source

T. Houck, D. Anderson,† S. Eylon,‡ G. Giordano,†
J-S Kim,‡ E. Henestroza,‡ S. Lidia,† L. Reginato,†
D. Vanecek,† G. Westenskow, and S. Yu,†

Lawrence Livermore National Laboratory, University of California
P. O. Box 5508, L-440, Livermore, California 94550, USA

†Lawrence Berkeley National Laboratory, University of California
Berkeley, California 94720, USA

‡Fusion and Accelerator Research
San Diego, California 92122 , USA

This paper was prepared to be submitted to
conference proceedings
RF96 Technologies for Linear Colliders Workshop, Hayama, Japan
April 7-12, 1996

April 11, 1996

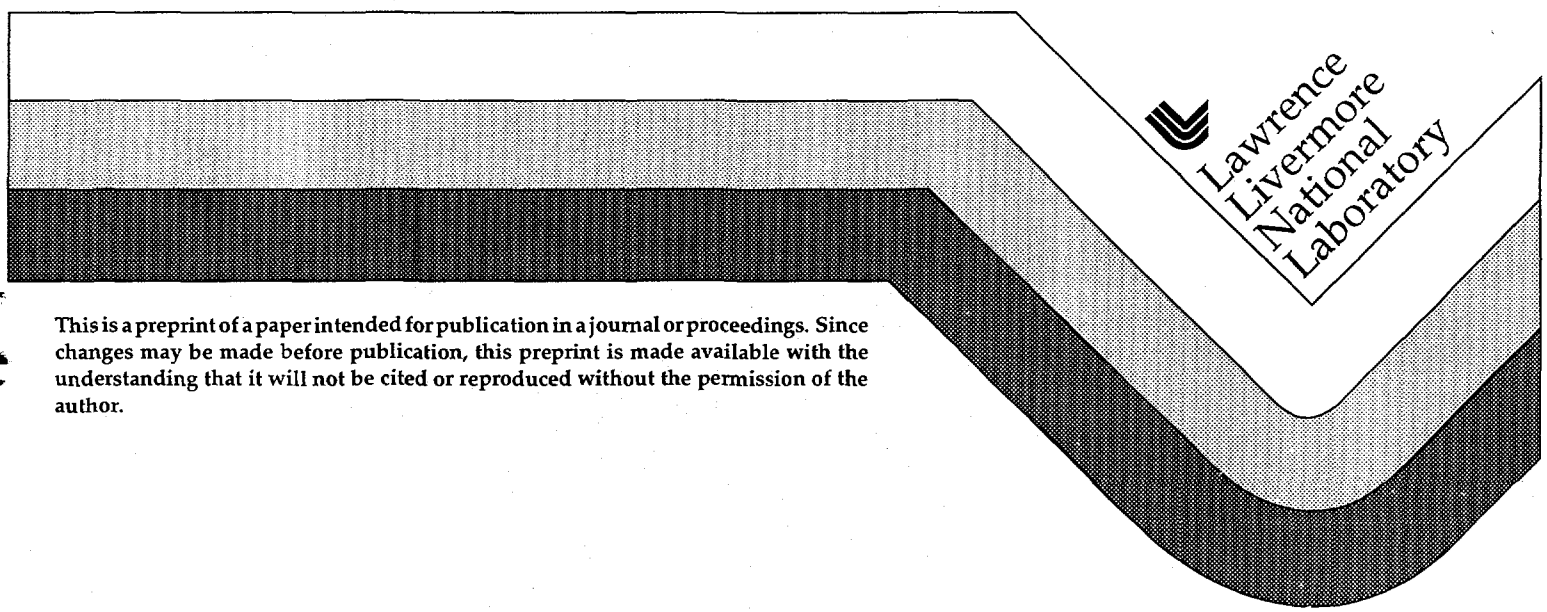

DISCLAIMER

RK-TBA Prototype RF Source*

T. Houck[1], D. Anderson, S. Eylon[2], G. Giordano, J-S Kim[2], E. Henestroza[2], S. Lidia, L. Reginato, D. Vanecek, G. Westenskow[1], and S. Yu

Lawrence Berkeley National Laboratory, 1 Cyclotron Road, Berkeley, CA 94720 USA,
[1]Lawrence Livermore National Laboratory, P.O. Box 808, Livermore, CA 94550 USA,
[2]Fusion and Accelerator Research, 3146 Bunche Avenue, San Diego, CA 92122 USA

Abstract. A prototype rf power source based on the Relativistic Klystron Two-Beam Accelerator (RK-TBA) concept is being constructed at the Lawrence Berkeley National Laboratory to study physics, engineering, and costing issues. The prototype is described and compared to a full scale design appropriate for driving the Next Linear Collider (NLC). Specific details of the induction core tests and pulsed power system are presented. The 1-MeV, 1.2-kA induction gun currently under construction is also described in detail.

INTRODUCTION

For several years a Lawrence Berkeley National Laboratory (LBNL) and Lawrence Livermore National Laboratory (LLNL) collaboration has been studying rf power sources based on the RK-TBA concept (1). This effort has included both experimental work (2) and theoretical studies (3). Last year, the collaboration prepared a preliminary design study for a rf power source suitable for the NLC (4,5). This design, referred to as the TBNLC, borrowed heavily from ongoing Heavy Ion Fusion (HIF) induction accelerator technology development (6), and specifically addressed issues related to cost, total system efficiency, and pertinent technical issues. For the 1-TeV center-of-mass energy design, the rf power source would be comprised of 50 RK-TBA subunits, each approximately 340 m in length with 150 extraction structures generating 360 MW per structure. We estimate that the conversion efficiency of wall plug energy to rf energy for this power source could be > 40%. Theory and simulations showed acceptable drive beam stability through the relativistic klystron, and no insurmountable technological issues were uncovered.

We have established a test facility at LBNL to verify the analysis used in the design study. The principle effort of the facility is the construction of a prototype of the proposed TBNLC rf power source, called the RTA (7). All major components of the TBNLC rf power source will be tested. However, due to fiscal constraints, the prototype will have only 8 rf extraction structures, with a possible upgrade to 12. Figure 1 shows a schematic of the RTA. Table 1 is a comparison between the pertinent parameters for TBNLC and the RTA prototype. As described below, the pulsed power system and induction cells in the extraction section will be very similar for both machines, allowing a demonstration of efficiency and establishing a basis for costing. Other features shared between the two machines include transverse chopping for initial beam modulation, adiabatic compression to increase the rf current component while accelerating the beam, a PPM quadrupole focusing system, and detuned rf extraction structures.

*The work was performed under the auspices of the U.S. Department of Energy by LLNL under contract W-7405-ENG-48, LBNL under contract AC03-76SF00098, and FAR under SBIR Grant DE-FG03-95ER81974.

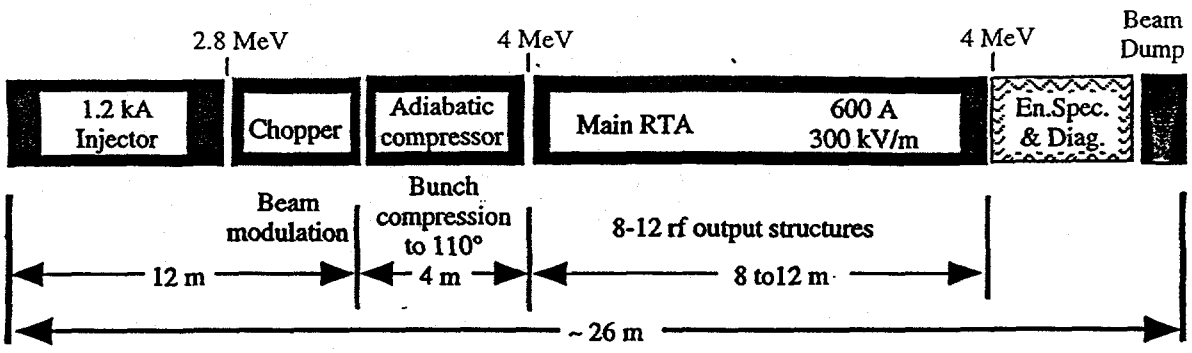

FIGURE 1. Schematic of the RTA showing major components.

The more important issues to be addressed by the RTA are efficiency, longitudinal dynamics, beam stability, emittance preservation and rf power quality. Efficiency can be separated into the conversion efficiency of wall plug power into beam power and beam power into rf power. The conversion of wall plug power into beam power can be fully measured in the RTA. High conversion efficiency of beam to rf power is only realized in a system with a large numbers of extraction structures. For the TBNLC, the number of extraction structures will be limited by beam stability and transport issues. The direct study of beam dynamics issues involving the beam transport through many tens of extraction structures will not be possible with the prototype. However, the reduced beam energy in the RTA extraction section permits the observation of almost an entire synchrotron period. Refer to equation (2). This will be sufficient to allow the beam to approach a steady state condition that can then be extrapolated to a full scale system. The verification of computer simulations used to model the beam dynamics in both the RTA and the TBNLC will be a high priority. Beam dynamics issues related to transverse modulation, misalignment of magnetic focusing systems, and adiabatic compression, e.g. emittance growth and corkscrew motion, can be adequately studied.

TABLE 1. Comparison between RTA and the TBNLC.

Parameter	RTA	TBNLC
Pulse Duration	200 ns	300 ns
Rise Time	100 ns	100 ns
Current		
Pre-Modulation	1,200 A	1,200 A
Extraction Section	600 A dc — 1,100 A rf	600 A dc — 1,150 A rf
Beam Energy		
Injector	1 MeV	1 MeV
Modulator	2.8 MeV	2.5 MeV
Extraction	4.0 MeV	10.0 MeV
Bunch Compression	240° – 110°	240° – 70°
Extraction Section PPM Quadrupoles		
Betatron Period	1 m	2 m
Lattice Period	20 cm	33.3 cm
Phase Advance	72°	60°
Occupancy	0.5	0.48
Pole Tip Field	870 G	812 G
Beam Diameter	8 mm	4 mm
RF Power		
Frequency	11.4 GHz	11.4 GHz
Power/Structure	180 MW	360 MW
Structures	Standing & Traveling-Wave	3 cell Traveling-Wave
Output Spacing	1 m	2 m

PULSED POWER SYSTEM

A significant factor in the TBNLC rf power source efficiency is the conversion of wall plug power into the induction drive beam power. Figure 2 is a schematic of an equivalent circuit of a pulse forming network (PFN) driving an induction accelerator cell. I_C is the core magnetizing current, I_B is the beam current, and I_N is any compensating network current. For optimum efficiency, I_N is minimized by designing the impedance of the PFN to match the nonlinear impedance of the induction core.

The efficiency of a TBA induction accelerator will depend on a number of factors. Beam transport dynamics will determine the size of the beam pipe and accelerating gradient. The rf power requirement will determine the pulse duration, beam current and repetition rate. Once these factors are established, the outer radius and material of the core can be calculated from:

$$\Delta V\, \Delta t = \Delta B\, A\, F_p, \qquad (1)$$

where ΔV is cell voltage swing, Δt is pulse duration, ΔB is core flux swing, A is core cross sectional area, and F_p is packing factor of the core material. Since the volume of core material increases nearly as the radius squared, smaller, more efficient and lower cost induction cells are obtained by using higher ΔB materials and minimizing the inner radius of the core.

Several core materials have been tested at the RTA Test Facility (8). METGLAS® alloys 2605SC and 2714AS, have been selected for use in the RTA. The alloy 2605SC has a ΔB of approximately 2.5 T with a core loss of about 2,000 J/m^3 for a 400 ns pulse (20 μm thickness). The alloy 2714AS has a lower ΔB, about 1.1 T, but a much lower core loss of about 150 J/m^3 (18 μm thickness) as shown in Figure 3. It is important that core tests are performed for the expected pulse shapes and durations to achieve accurate loss measurements. This effect is illustrated in Figure 4 where core losses for both materials are plotted as a function of rate of flux swing, dB/dt. For our proposed TBNLC geometry, the low core loss 2714AS can achieve substantial improvement in efficiency over 2605SC.

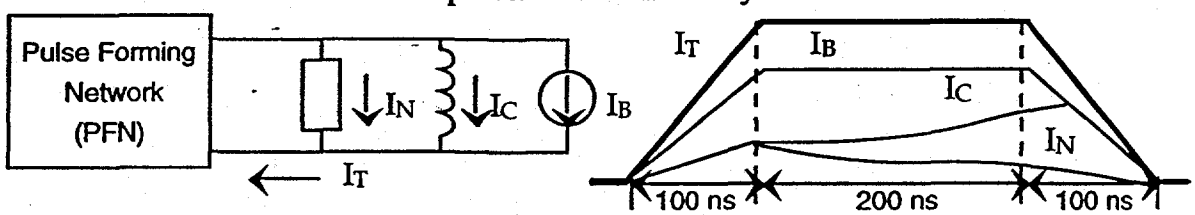

FIGURE 2. Equivalent circuit of an induction cell.

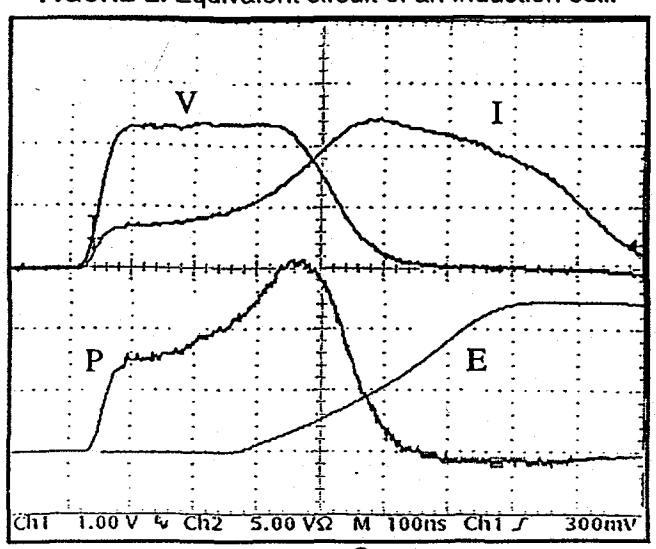

FIGURE 3. Oscilloscope traces for pulsed METGLAS® alloy 2714AS core. Time scale: 100 ns/div. V is applied voltage (1 kV/div), I is current dissipated in core (50 A/div), P is power (VI, 50 kW/div), and E is energy (time integrated power, 20 mJ/div, 250 ns offset). Total energy dissipated = 47 mJ or 150 J/m^3.

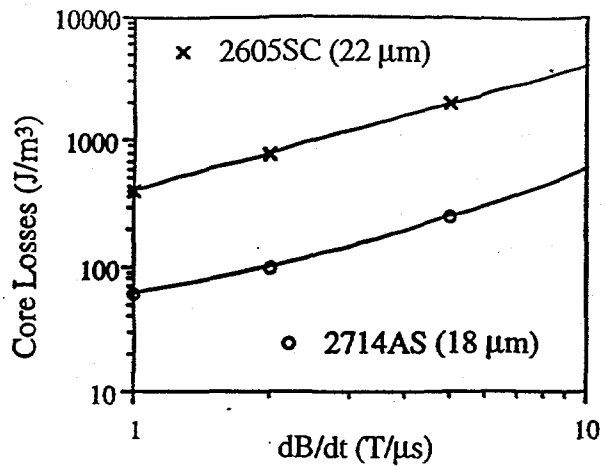

FIGURE 4. Core loss for different rates of magnetic flux change.

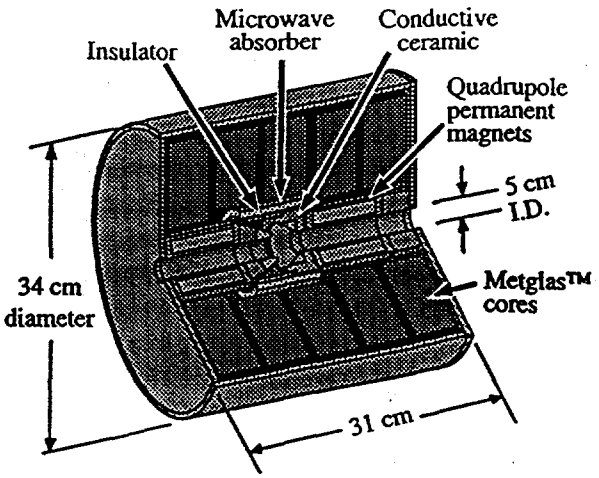

FIGURE 5. Proposed RK-TBA induction cell design with five cores per cell.

We have also realized an efficiency enhancement in our power modulator technique. The modest repetition rate (120 Hz) and current rise time (100 ns) envisioned for the NLC permits the use of a simple, and cost effective thyratron driven modulator. The total induction cell core is then segmented into smaller cores each individually driven at no more than 20 kV. Driving at this voltage level avoids separate step-up transformers and can be generated directly by a thyratron with 40 kV charging voltage on the PFN. A proposed induction core design is shown in Figure 5. Geometrical constraints due to location of magnets, rf extraction structures, and pumping ports, as well as accelerating gap fields, determine the number of cores per induction cell. The TBNLC design has five cores per cell while the RTA will have three cores. Both designs use standard 2" wide METGLAS® ribbon. In our design, the PFN charging current flows through the induction core resetting the core prior to the next acceleration cycle.

Beam energy flatness is an important issue affecting both beam transport and rf phase variation. As shown in Figure 3, the current drive to the cores becomes nonlinear for a constant amplitude voltage pulse. The nonlinearity is a result of the core saturating from the inner radius outward. The generated voltage amplitude can be kept constant, within bounds, during the initial stages of core saturation simply by tapering the impedance of the PFN stages. The PFN will consist of many coupled L-C stages with impedances adjusted to temporally match the induction core impedance. The aspect ratio ($\Delta r/\Delta z$) of the individual cores strongly influences the saturation behavior. Low aspect ratio cores saturate rapidly across their cross section requiring less impedance tapering.

We may use two different pulsed power systems for the RTA. The adiabatic compressor and extraction sections will use induction modules and a pulsed power system very similar to those proposed for the TBNLC. This part of RTA will be used to verify efficiency, technical aspects, and cost figures determined in the TBNLC design study. The combination of the low loss METGLAS® alloy 2714AS cores and the thyratron driven modulators will result in a conversion efficiency of wall plug power to beam power of 59%. The injector will use METGLAS® alloy 2605SC for greater flux swing, and possibly separate step-up transformers.

INJECTOR

The injector consists of two sections, a 1-MV, 1.2 kA induction electron source, referred to as the gun, followed by several induction accelerator cells to boost the energy to 2.8 MeV. Two main goals of the injector design are minimizing electrical field stresses in the gun and

realizing the lowest possible emittance growth. Development tests of the pulsed power system on a test core indicated that the geometry of the existing SNOWTRON induction injector cells would not produce a satisfactory voltage pulse, both in amplitude flatness and volt-seconds. Figure 6 is an illustration of our new gun design. The cores are segmented radially to reduce the individual aspect ratios with each driven separately at about 14 kV. We chose a constant radius design for the cathode-side cells. The added METGLAS® core cost due to the 10% increase in total core volume was recovered in reduced insulator and fabrication costs. The components of the induction cells for the cathode-side of the gun are in fabrication and we expect to do a pulsed power test, no beam, on this half of the injector by September 1996.

A novel feature of the gun design is the insulator. We will do initial high voltage testing with a single, 30 cm ID, PYREX® tube for the insulator with no intermediate electrodes. Average gradient along the insulator at the operating voltage of 500 kV is about 5.1 kV/cm. Maximum fields at the triple points, intersection of insulator, vacuum, and metal, is less than 3.5 kV/cm. Maximum surface fields in the cathode half of the gun are about 85 kV/cm. Figure 7 shows the results of Poisson runs for high field regions near the back of the cathode. The rational for using PYREX® is to explore methods of reducing the costs of induction injectors. PYREX® is significantly less expensive than ceramic, and additional savings are realized by avoiding intermediate electrodes. There is additional risk associated with this approach. However, our design allows for the addition of intermediate electrodes and/or substitution of a ceramic insulator with minimal impact to schedule or expense. The PYREX® design will be tested on the cathode half of the gun before we are committed to the anode insulator.

We would like to use existing ETA II induction cells for the accelerator section (following the gun). The cores in each induction cell of the accelerator section may be driven as a single unit to maximize the available cross sectional area. A pulsed power system demonstration with a test cell will be accomplished before finalizing the accelerator induction cell design. Driving multiple cores will require the use of a step-up transformer to deliver the required 80 to 100 kV per cell. The core material for the injector, both gun and accelerator section, will be METGLAS® alloy 2605SC to maximize the flux swing. Here, the issue is generating the required volt-seconds within the geometrical constraints of exisitng components.

The solenoidal field configuration must be optimized for the injector to control the beam radius while minimizing emittance growth. The present electrode package will be used during initial testing. However, a new electrode package and larger dispenser cathode are required to produce the desired low-emittance 1.2-kA, 1-MeV electron beam. Figure 9 shows an EGUN simulation of the beam radius and normalized edge emittance through the injector. The design

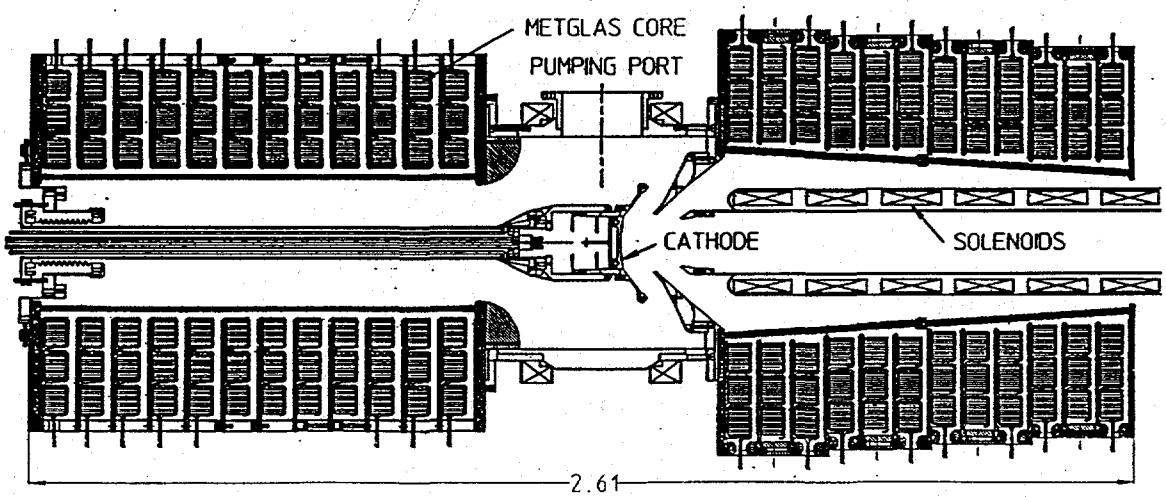

FIGURE 6. Illustration of the 1-MV, 1.2-kA, induction gun design.

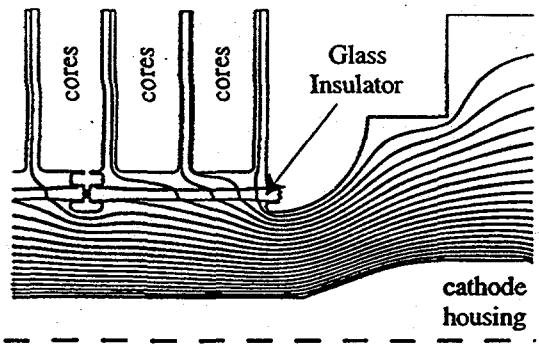

FIGURE 7. Poisson simulations of the field in the area behind the cathode holder.

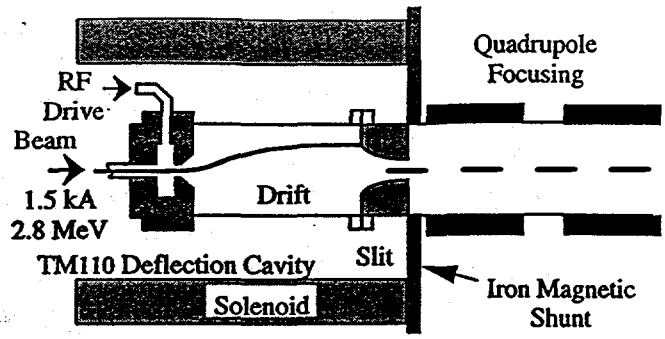

FIGURE 8. Schematic of the RTA beam modulator (chopper).

goal is for a beam radius < 5 mm and ε_N < 250 π-mm-mr at the chopper entrance. Alignment of the focusing solenoids is critical to avoid corkscrew motion and emittance growth in the injector. The focusing solenoids in the gun are located in the anode stalk. Homogenizer rings (9) are being considered for the anode stalk. This could eliminate the need for correction coils and simplify alignment.

For the accelerator section, a stretched wire alignment scheme (10) will be used to determine the offset of the solenoid's magnetic axis from a reference mechanical axis for each cell. From past experience, the resolution of this alignment scheme to offset errors is approximately ± 0.05 mm. Each cell also contains a steering (sine/cosine) coil to correct for tilt errors. The required tilt correction will also be determined. The entire alignment will be performed in a precision mill with tolerance on the order of tenths of a mil. A fiduciary will be placed on the outer case of the cell to permit alignment of the magnetic axis when the cells are mounted on the strongback. With this procedure, we expect solenoid offset errors of less than ± 0.08 mm and negligible tilt errors.

Experience operating the ETA II accelerator has shown that careful alignment of the solenoids is not sufficient to reduce the amplitude of the corkscrew motion (11,12) to the 0.5 mm desired for the RTA injector. Individual adjustments of the induction cells will permit improved solenoid alignment in the RTA. However, we anticipate using a time independent steering algorithm (13) developed for ETA II to control steering coils on the solenoids. This algorithm corrects for the Fourier component at the cyclotron wavelength of the field error, and led to an order of magnitude reduction in the corkscrew amplitude of the ETA II beam.

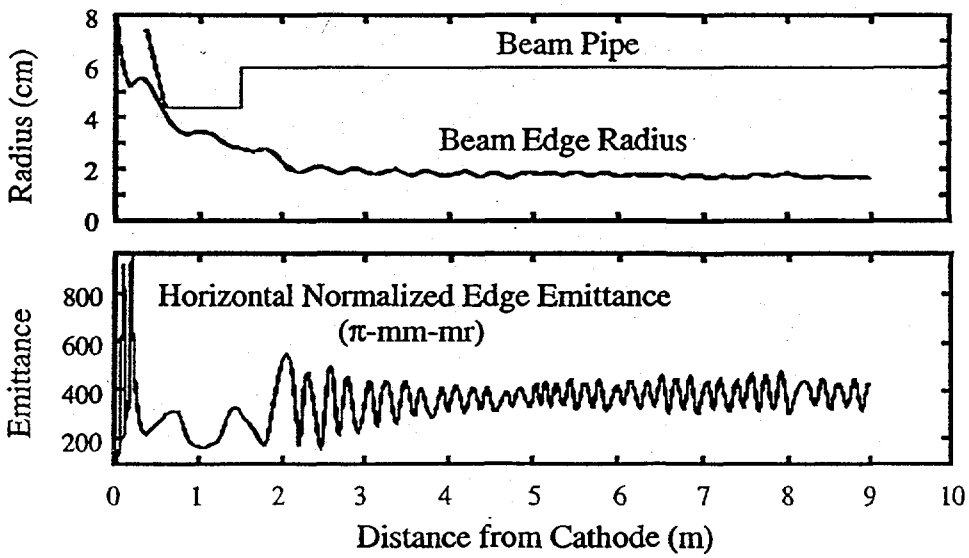

FIGURE 9. EGUN simulations of beam transport and edge emittance through the injector.

BEAM MODULATION

A transverse chopping technique will be used for the initial modulation of the beam. The modulator section of the Choppertron (14), a 11.4 GHz rf generator, has been refurbished for this purpose. A schematic of the modulator is shown in Figure 8. The solenoidal field immersed incoming electron beam is deflected in the horizontal plane by a 5.7 GHz TM_{110} deflection cavity causing the beam to describe semi-helical trajectories along the drift space. The beam scans in a vertical plane across an on-axis aperture placed a quarter betatron wavelength after the deflection cavity. Thus, the 5.7 GHz spatially modulated dc beam incident on the aperture becomes a phase coherent, amplitude modulated beam at 11.4 GHz.

The desired bunch length, peak current, and energy for the drive beam in the extraction section of the prototype is respectively 110 degrees, 600 A, and 4 MeV. Such a train of bunches could be generated by directly chopping the unmodulated beam. However, considerations of efficiency (70% of the beam would be lost) and practical feasibility (we expect approximately 1.2 kA of peak current from the injector) require that we do not fully modulate the beam by chopping. Our intent is to "chop" the beam at an energy of 2.8 MeV into bunches of approximately 240 degrees. An adiabatic compressor section will be used to further bunch and accelerate the beam.

Designs of chopper systems have been extensively analyzed (15,16) and the original Choppertron was optimized for operation with the ETA II induction beam. The intent for the prototype experiment is to limit modifications of the modulator section of the Choppertron to adjustments in the drift length and the chopping slit aperture size. It is desirable for the radius of the beam to remain relatively constant in the chopper. For a given beam energy, current, and emittance, the radius is determined by the solenoidal field. Once the solenoidal field is determined for the desired beam radius, the drift section length is also fixed. The maximum deflection amplitude at the aperture is determined by the transverse momentum imparted to the beam by the deflection cavity. The deflection amplitude and chopping slit aperture determine the emittance growth and the modulated beam's characteristics. In our design, the beam is deflected sufficiently to deposit about 45% of the current on the surface of the aperture. Thus the beam fills the acceptance of the aperture. A smaller aperture leads to smaller emittance, but also limits the current transmitted. With a 10 mm aperture at a drive power of about 0.8 MW, the emittance is increased approximately 70% and the dc current component is 660 amperes with about 500 amperes of rf current.

The desired beam characteristics at the entrance of the extraction section are achieved with adiabatic compression. In the adiabatic compressor, the bunch length is reduced from 240° to 110° with standing-wave idler cavities while the beam is accelerated to an energy of 4 MeV. The accelerating gradient of the induction cells (300 kV/m) establishes the minimum length of the adiabatic compressor at 4 meters. Extensive 1D numerical studies have been performed to determine the most efficient scheme for bunching the beam. The present design uses seven idler cavities appropriately spaced and detuned to progressively bunch the beam. The idler cavity is designed with a resonant frequency higher than the drive frequency. Appropriate design and spacing of the idler cavities can eventually bunch the bucket to the desired length. Important parameters of the adiabatic compressor are summarizes in Table 2.

RF POWER EXTRACTION

After leaving the adiabatic compressor, the beam enters the extraction section. Here the beam energy is periodically converted into rf energy (via extraction cavities) and restored to its initial value (via induction modules). Stable propagation of the rf bucket during transit

TABLE 2. Parameters of the Adiabatic Compressor.

cavity	position (m)	bunch length (degrees)	Beam Energy E_k (MeV)	resonant frequency (GHz)
1	0.0	240	2.8	11.82
2	0.6	229.7	2.98	11.82
3	1.2	217.9	3.17	11.82
4	1.8	201.7	3.36	11.74
5	2.4	177.6	3.53	11.74
6	3.0	148.6	3.69	11.74
7	3.6	122.0	3.85	11.74
exit	4.0	105.5	4.00	

through many resonant cavities and achievable rf power extraction have been studied numerically. Space charge effects and energy spreads due to rf fields in the extraction structures tend to debunch the beam as it traverses the extraction section resulting in reduced power extraction in subsequent extraction structures. To counteract this effect, inductively detuned extraction structures are used.

Both traveling wave (TW) and standing wave (SW) structures are being considered for the extraction section of the RTA. The TBNLC design used TW structures to reduce the surface fields associated with generating 360 MW per structure (See Figure 10). RTA is designed to generate 180 MW per structure. Thus, inductively detuned SW cavities are a practical alternative. We have used SW cavities in our modeling to perform complete 2D simulations and to validate the inductive detuning concept. The detuning concept for the SW extraction cavities is similar to that used in the adiabatic compressor cavities. The required detuning is also affected by the finite external Q of the cavities. Different cavities can have different Q values to optimize the output power and the bunching. The detuning mechanism is required for stable rf power production through the extraction section. Figure 11 shows simulation results of detuning where the resonant frequency of the detuned structures is 11.566 GHz.

An alternative design for the extraction cavity based on Shintake's choke mode cavity (17) is shown in Figure 12. The motivation for this design is damping of the beam-induced higher-order modes (HOM). The HOMs are heavily damped through the radial transmission lines terminated in matched loads, while the fundamental mode is established by means of an imaginary short due to the choke structures. The fabrication time and cost for the choke mode cavities should be minimal due to their cylindrical geometry.

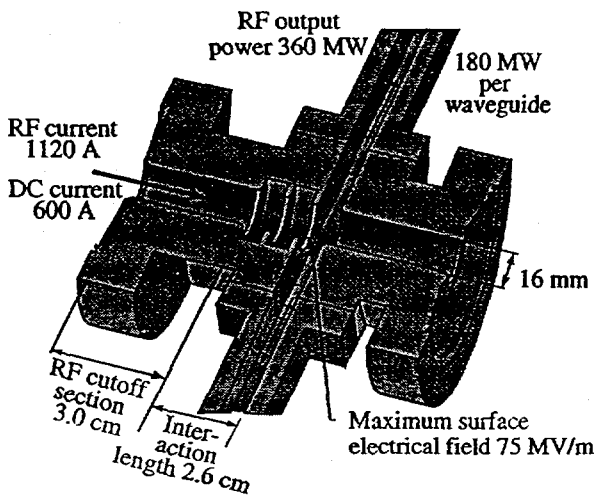

FIGURE 10. Illustration of an extraction structure design for the TBNLC.

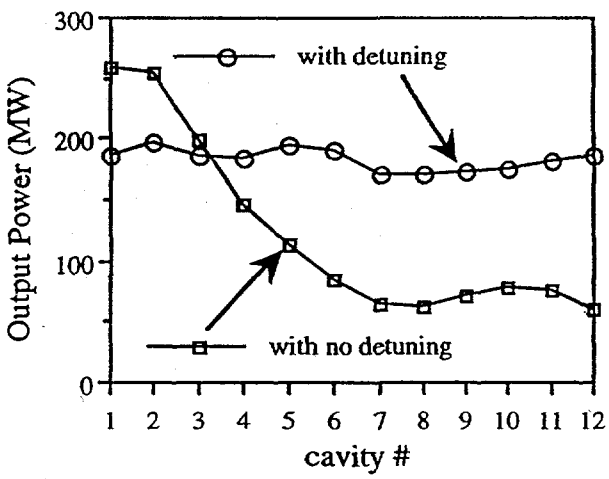

FIGURE 11. Simulations of rf power generated per output, with and without cavity detuning

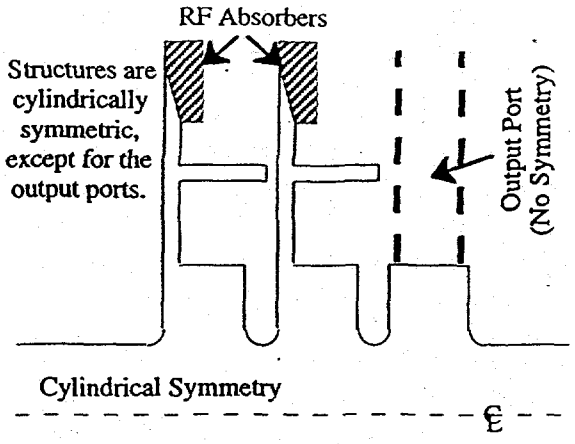

FIGURE 12. Sketch of a three-cell extraction structure configured with choke mode cavities.

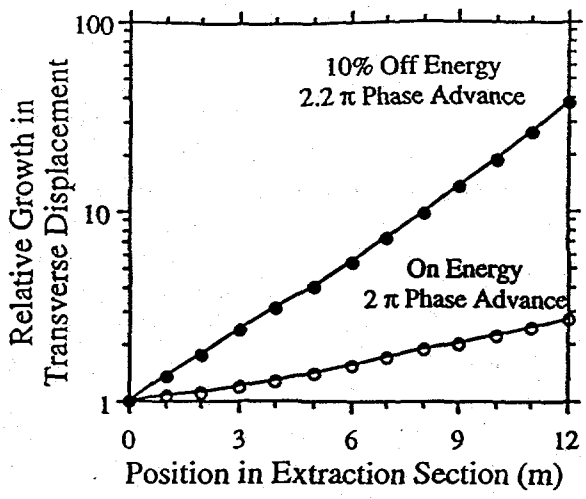

FIGURE 13. Simulation results showing the growth in the transverse displacement of the beam centroid due to HOM deflection in the rf structures.

BEAM DYNAMICS ISSUES

Transverse instability of the beam due to the excitation of HOMs in the rf extraction structures and induction cell gaps is a serious issue for a long relativistic klystron. We do not anticipate beam loss due to the HOM excitation, but the effect should be measurable. The HOM's associated with three different components will predominate in the prototype. Fortunately, the frequency ranges do not overlap so that the effects can be studied separately.

The first is the approximately 300 MHz transverse mode in the accelerator induction cells. ETA II has operated with 3 kA of current through 60 induction cells of the same geometry, but with ferrite cores. The 20 accelerator cells in the RTA should not poise an instability problem with 1.2 kA of current, but it should be possible to detect small beam oscillations at 300 MHz by the use of rf probes.

Of greater concern are the 60 to 80 prototype induction cells of the adiabatic compressor and extraction section. The transverse impedance of a cell is roughly proportional to the cell gap divided by the square of the beam pipe radius. The transverse impedance of the smaller prototype cells is about four times that of the larger accelerator cells. Numerical simulations of the growth in the transverse instability indicated a twelve-fold increase in centroid movement over 80 induction cells from an initial seed disturbance for a monoenergetic beam. Imposing a ± 5% energy spread on the beam produced only a four-fold increase in the simulated centroid motion due to the effect of Landau damping. The interaction of the beam with the rf structures was not included in these simulations. A factor of 100 increase in growth from a noise signal is expected to be tolerable.

The third and most critical instability affecting transverse motion is caused by the rf output structures in the extraction section. Despite heavy damping of the structures and the effect of Landau damping, it was necessary to use the "Betatron Node" scheme (18) to suppress the transverse instability to a tolerable level for the TBNLC. In the "Betatron Node" scheme, the extraction structures are placed a betatron wavelength apart so that a deflected beam will return to the same transverse position at the following structure. Simulation results of the transverse instability growth through the extraction section are shown in Figure 13. The rf characteristics of the three-cell traveling wave output structures described in the TBNLC design study were used for the simulation ($Z_\perp/Q = 3\Omega$ per cell, dipole resonant frequency of 14 GHz, Q = 10 for first and third cells and 3,500 for second, and dipole phase advance of

about $2\pi/3$). For the simulation a monoenergetic beam increasing from 0 to 600 A in 50 ns and total pulse duration of 200 ns was used. A step function offset was used as the excitation seed. A relative small change in the beam energy from that required for the "Betatron Node" scheme can lead to substantial increase in the growth of the instability as indicated in Figure 13. While the growth remains tolerable for both cases shown, the idler cavities in the adiabatic compressor require different transverse rf characteristics than the extraction output cavities to avoid beam loss and/or adverse emittance growth. The difference in HOM power generated in the cavities is three orders of magnitude greater after 12 cavities when operating at an energy 10% above the optimum for the "Betatron Node" scheme. A measurement of the HOM component in the output power is expected to be sensitive to the effectiveness of the scheme.

Longitudinal stability issues include both the rf bucket and the phase relationship between rf buckets. The rf bucket must remain appropriately bunched for stable rf current and power extraction. Simulation results of the rf power generated and bunching in the extraction section when the resonant frequency of all the detuned output structures has been set to 11.566 GHz are shown in Figure 11. The length of RTA is adequate for a meaningful measurement of the longitudinal beam dynamics involved in the detuning of the output structures to maintain the rf bucket. The synchrotron wavelength can be approximated as:

$$\lambda_s = 2\pi \left(\frac{\omega}{c\,\gamma^3} \frac{d\gamma}{dz} \right)^{-1/2}. \qquad (2)$$

At 4 MeV, accelerating gradient of 300 kV/m, and 11.4 GHz, λ_s is $\approx$ 14 meters.

Numerical sensitivity studies indicate that rf output power is insensitive to energy variation and shows small variations (< 4%) for current variations of ± 1%. The variations were imposed for the flat-top portion of the beam pulse. Phase stability is not appreciably effected by current variations of less than ± 1%. However, phase sensitivity leads to a severe requirement on the average (head-to-tail) energy variation for the flat-top portion of the beam pulse. Phase variations are modeled well by the following first order formula:

$$\frac{\Delta\varphi}{\Delta z} = \frac{k}{\bar{\gamma}^3} \Delta\gamma, \qquad (3)$$

where $\Delta\varphi$ is phase variation, $\Delta\gamma$ is head-to-tail energy variation over the pulse length, k is the free space wave number, and $\bar{\gamma}$ is the average beam energy. With the RTA parameters, assuming that field phase variation should not exceed ± 5°, the required pulse energy flatness (flat top) is estimated to be ± 0.3 % for an 8-m extraction section.

Beam emittance is an important parameter for the RTA. After the chopper, the focusing system is comprised of permanent quadrupole magnets. The ppm quadrupole focusing is important in the TBNLC design for cost and efficiency reasons. For the RTA, mechanical design constraints and the experimental goal of studying the "Betatron Node" scheme require a pole field at a radius of 2 cm for the quadrupoles of about 870 gauss, a half lattice period of 10 cm, occupancy factor of 0.5, and a phase advance of 72°. The normalized edge emittance must be no larger than 800 π-mm-mr to meet the design goal of an average beam radius (edge) in the extraction section of 4 mm.

Our goal is to limit the emittance growth in the injector from beam optics to a factor of three times the thermal source emittance of about 80 π-mm-mr (0.1 eV) for the cathode. The chopper is expected to increase the emittance by a factor of about 1.7. Thus it is very important to minimize sources of emittance growth such as non-zero magnetic flux at the cathode, magnet misalignments, solenoid to quadrupole matching, and higher order multipoles in the quadrupole magnets. The strong focusing used in the extraction section and the large beam energy spread will convert any transverse motion of the beam, e.g. corkscrew motion or transverse instabilities, into an increase in effective emittance.

SUMMARY

We have started construction on a prototype rf power source based on the RK-TBA concept, called the RTA. Testing of material for the induction cores has been completed and two METGLAS alloys selected for use in the RTA. The pulsed power system for the gun has been design and is based on driving individual cores at about 14 kV using glass thyratron tubes switching at 28 kV. The pulsed power system design for later portions of the RTA will continue to develop during the testing of the gun. A novel feature of the gun is the use of PYREX® tubes as 500 kV insulators. Satisfactory performance of the PYREX® insulator would demonstrate an inexpensive alternative to the more standard graded, ceramic insulator.

The RTA will be used to study physics, engineering, and costing issues involving the application of the RK-TBA concept to linear colliders. All major components of a rf power source suitable for driving the NLC can be studied including the pulsed power system, current modulating system, ppm quadrupole focusing, and detuned rf extraction cavities. Some of the more important issues that the RTA will address are efficiency, longitudinal beam dynamics, beam stability, emittance preservation, and rf power quality.

ACKNOWLEDGMENTS

We thank Andy Sessler and Swapan Chattopadhyay for their support and guidance. Craig Peters provided mechanical engineering support. Bill Abraham and Ken Leach provided electrical design support. Yu-Jiuan Chen and George Caporaso provided valuable assistance with the induction accelerator design.

REFERENCES

1. Sessler, A.M. and Yu, S.S., "Relativistic Klystron Two-Beam Accelerator," *Phys. Rev. Lett.* 54, 889 (1987).

2. Westenskow, G.A., and Houck, T.L., "Relativistic Klystron Two-Beam Accelerator," *IEEE Trans. on Plasma Sci.*, 22, 750 (1994).

3. Giordano, G., et al., "Beam Dynamic Issues in an Extended Relativistic Klystron," in *Proc. of the 1995 IEEE Particle Accelerator Conf.*

4. Yu, S.S., et al., "RK-TBA Based Power Source for a 1 TeV NLC," LBID-2085/UCRL-ID-119906, Berkeley, Lawrence Berkeley National Laboratory, Feb. 1995.

5. Loew, G.A., and Weiland, T., *International Linear Collider Technical Review Committee Report 1995*, Stanford, Stanford University, 1995, pp. 61–65, 83, 84.

6. Yu, S.S. "Induction Accelerators and Injectors for Heavy Ion Fusion," in *Proc. of the 1995 IEEE Particle Accelerator Conf.*

7. Houck, T.L., and Westenskow, G.A., "Prototype Microwave Source for a Relativistic Klystron Two-Beam Accelerator" to be published in *IEEE Trans. on Plasma Sci.*

8. Reginato, L., et al., "Engineering Conceptual Design of the Relativistic Klystron Two-Beam Accelerator Based Power Source for 1-TeV Next Linear Collider," in *Proc. of the 1995 IEEE Particle Accelerator Conf.*

9. Feinberg, B., et al., "A Method for Improving the Quality of the Magnetic Field in a Solenoid," *Nucl. Instr. and Meth.*, 203, pp. 81–85 (1982).

10. Griffith, L.V., and F.J. Deadrick, "Progress in ETA-II Magnetic Field Alignment Using Stretched Wire and Low Energy Electron Beam Techniques," *Proc. of the 1990 LINAC Conf.*, pp.423–425.

11. Chen, Y-J, "Corkscrew Modes in Linear Accelerators," *Nucl. Instr. and Meth.*, A292, pp. 455–464 (1990).

12. Allen, S.L., et al., "Measurements of Reduced Corkscrew Motion on the ETA-II Linear Induction Accelerator," *Proc. of the 1991 IEEE Particle Accelerator Conf.*, pp. 3094-3096.

13. Chen, Y-J, "Beam Control in the ETA-II Linear Induction Accelerator," *Proc. of the 1992 LINAC Conf.*, pp. 540-544.

14. Haimson, J. and Mecklenburg, B., "Design and Construction of a Chopper Driven 11.4 GHz Traveling Wave RF Generator," *Proc. of the 1989 IEEE Particle Accelerator Conf.*, 89CH2669, pp. 243-245
15. Haimson, J., "Injector and Waveguide Design Parameters for a High Energy Electron-Positron Linear Accelerator," *IEEE Trans. Nucl. Sci.*, NS-12 No. 3, pp. 499-507, 1965.
16. Haimson, J., "High Duty Factor Electron LINACS," in *Linear Accelerators*, eds. P.M. Lapostolle and A.L. Septier, (North-Holland, Amsterdam, 1970), pp.462-466.
17. Shintake, T, "The Choke Mode Cavity," *Jpn. J. Appl. Phys.* 31, pp. L1567–L1570, 1992.
18. Li, H., et al., "Design Considerations of Relativistic Klystron Two-Beam Accelerator for Suppression of Beam-Breakup," in *SPIE Proceedings* Vol. 2154-10, 1994.

Technical Information Department · Lawrence Livermore National Laboratory
University of California · Livermore, California 94551